COHERENT STRUCTURES AND SUBFILTER-SCALE DISSIPATION IN LES: A FIELD STUDY

Matthew A. Carper* and Fernando Porté-Agel
Saint Anthony Falls Laboratory
University of Minnesota, Minneapolis, Minnesota

1. INTRODUCTION

The success of large-eddy simulation (LES) of the atmospheric boundary layer (ABL) relies on the ability of the subfilter-scale (SFS) models to reproduce the effects of the unresolved (subfilter) scales on the dynamics of resolved scales accurately. Recent *a priori* experimental studies have been crucial to improving our understanding of SFS physics (e.g. Porté-Agel *et al*, 2001a,b; Sullivan *et al*, 2003; Kleissl *et al*, 2003). There is still, however, a lack of information on the specific role that three-dimensional coherent structures play on the local transfers of energy and temperature variance between resolved and subfilter (unresolved) scales relevant to LES of the ABL.

The quantities that require modeling in LES are the subfilter-scale (SFS) fluxes and stresses,

$$q_i = \widetilde{u_i\theta} - \tilde{u_i}\tilde{\theta} \quad \text{and} \tag{1}$$

$$\tau_{ij} = \widetilde{u_i u_j} - \tilde{u_i}\tilde{u_j}, \tag{2}$$

respectively, where the tilde (˜) denotes a spatially filtered (at scale Δ) variable. The effects of these stress/fluxes on the resolved flow variables can be studied by considering the SFS dissipation rate (transfer rate between resolved and subfilter scales) of scalar variance and energy,

$$\chi = -q_i \frac{\partial \tilde{\theta}}{\partial x_i}, \tag{3}$$

$$\Pi = -\tau_{ij}\tilde{S}_{ij} \tag{4}$$

where $\tilde{S}_{ij} = \frac{1}{2}(\frac{\partial \tilde{u_i}}{\partial x_j} + \frac{\partial \tilde{u_j}}{\partial x_i})$ is the filtered strain rate tensor. These SFS dissipation rates have special importance since accurately reproducing their mean values has been found to be a necessary condition for LES to yield correct flow statistics (Meneveau and Katz, 2000).

In this paper, we present results from a field study designed and carried out to compute the above SFS quantities and study, via conditional averaging, the relation of strong positive (forward-scatter) and negative (backscatter) SFS dissipation events to local features of the flow. A three-dimensional conceptual model of the flow around strong positive and negative SFS dissipation events is presented that summarizes our findings. The effect of atmospheric stability on the inclination of these structures is also addressed.

2. EXPERIMENTAL DATA

The field study took place at the Surface Layer Turbulence and Environmental Science Test (SLTEST) facility located on the salt flats in the Great Salt Lake Desert of Western Utah during July, 2002. The experimental setup consists of 16 sonic anemometers used in an arrangement with a 6 m-high vertical array (10 anemometers) that intersected a 3 m-wide horizontal array (7 anemometers). Fig. 1 shows a schematic of the setup. Data-sets were selected based from 30-minute periods with stationary flow and angles of incidence (β in Fig. 1) smaller than 35°. Most of the results presented here correspond to one data-set characterized by an stability parameter of $z/L = -0.24$ (where z is the sensor height and L is the Obukhov length).

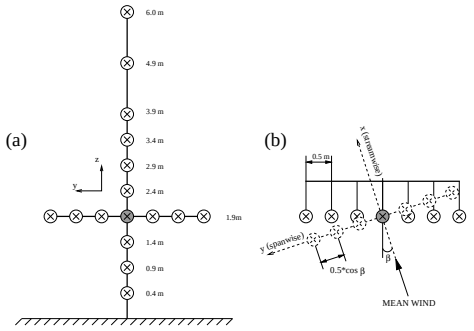

FIG. 1: Schematic of the (a) front view and (b) top view of the experimental setup. The heights of the sensors are indicated in (a) and the alignment of the wind relative to the anemometers are depicted in (b). The shaded circle represents the position at which SFS dissipation rates were estimated.

SFS fluxes (q_i, Eq. 1) and stresses (τ_{ij}, Eq. 2) are computed using a one-dimensional streamwise filter with a width of Δ = 2.0 m in the streamwise direction (applying Taylor's hypothesis). The gradients of the filtered velocity and temperature are computed along all three axial directions at the location where the vertical and horizontal arrays intersect using a centered finite-differencing scheme (again using Taylor's hypothesis). The SFS dissipation rates of scalar variance and energy are then calculated. The probability density function (PDF) of χ and Π are shown in Fig. 2 and exhibit large intermittency with numerous occurrences of backscatter (negative values). The non-Gaussian behavior of these SFS transfers is problematic to modeling.

3. SFS DISSIPATION EVENTS AND COHERENT STRUCTURES

Previous field studies by Porté-Agel *et al* (2001a,2001b) have related sweep and ejection events with positive and negative SFS dissipation rates of scalar variance in the ABL and studied the effect of filter scale and atmospheric

*Corresponding author address: M.A. Carper, Saint Anthony Falls, 2 3rd Avenue SE, Minneapolis, MN 55414, e-mail: carper@msi.umn.edu

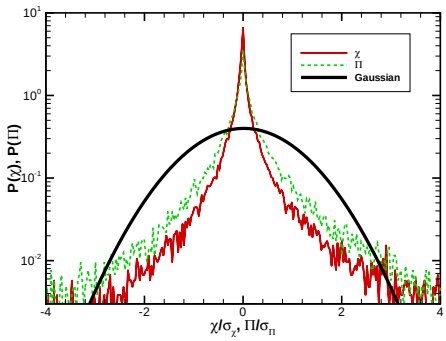

FIG. 2: Probability density functions of the SFS dissipation rate of scalar variance, χ, and SFS dissipation rate of resolved energy, Π. The thick solid line represents the Gaussian distribution.

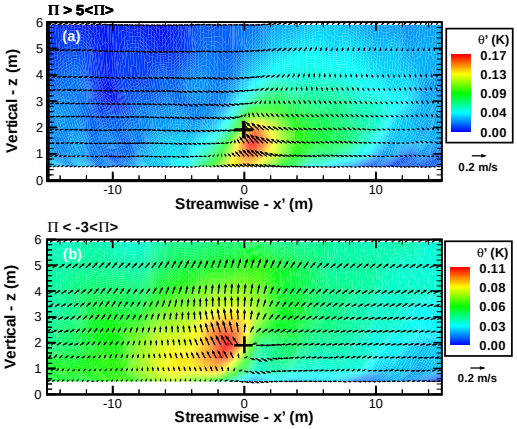

FIG. 3: (a) Vertical fields of conditionally averaged temperature fluctuations, θ' (K), with overlaid conditionally averaged fluctuating velocity vectors for (a) positive and (b) negative SFS dissipation rates of energy under weakly-unstable conditions. Flow is from left to right and every other vector in the streamwise direction has been removed for visual purposes. The '+' indicates the location at which the SFS dissipation rates satisfy the threshold condition.

stability on SFS physics. The local flow conditions that contribute to significant positive and negative SFS dissipation rates are studied here by conditionally sampling flow properties (temperature, velocity and vorticity) based on strong (positive or negative) events of χ and Π. Data from the same time period used in Fig. 2 (z/L = -0.24) is used here. Two-dimensional windows (from the horizontal and vertical arrays) of data (temperature, velocity and vorticity) surrounding locations where these extreme events occur are sampled and averaged together. Further details of this type of conditional-averaging procedure can be found in Porté-Agel *et al* (2001a,b) and Carper *et al* (2004).

The vertical field of conditionally averaged temperature based on strong-positive SFS dissipation rates (forward-scatter) of energy is presented in Fig. 3a. Positive SFS dissipation events (at the location marked with a '+' in Fig. 3a) tend to occur at the interfaces of relatively warmer air (from below) and cooler air (from above). The fluctuating-velocity-vector field (also conditionally averaged) shows that near the forward-scatter events there is typically a convergence of the flow with the inception of an ejection (velocity directed upwind and away from the surface) below the event location. For strong-negative SFS dissipation rates (backscatter, see Fig. 3b), the events tend to take place at a divergence in the flow with a volume of warm air being ejected away from the event location. Seemingly, Figs. 3(a) and 3(b) suggest that different regions surrounding an ejection of relatively warmer air appear to be associated with completely opposite signs of SFS dissipation. The results of the conditional averages based on either the SFS dissipation rate of energy (Π, Fig. 3) or the SFS dissipation rate of scalar variance (χ, not shown) support the same conclusions regarding the local flow properties around strong-positive and strong-negative SFS dissipation events. This is also true for the other conditionally averaged fields shown below, and therefore, only results corresponding to SFS dissipation of energy are presented here.

Next, the conditional averaging procedure is applied to the vorticity fields to obtain a clearer picture of the 'average flow structure' associated with strong forward and backward scatter events. The vertical field of conditionally averaged vorticity (spanwise component only) corresponding to the strong-positive SFS dissipation rates (Figs. 4a) shows a region of vorticity which is inclined downwind (at approximately 15-20°) with a core of vorticity located downwind and above the SFS dissipation events. The conditionally averaged flow field surrounding the backscatter events (Figs. 4b) also has a core region of positive vorticity. However, in this case it is located upwind and above the SFS dissipation events.

To better understand the three-dimensionality of the flow structures surrounding these SFS dissipation events, horizontal fields of conditionally averaged temperature and vorticity (vertical component only) are calculated corresponding to the same SFS dissipation events used to conditionally average vertical fields. The horizontal fields of conditionally averaged temperature are presented in Fig. 5. These results show that strong forward-scatter (Fig. 5a) and backscatter (Fig. 5b) occur, respectively, downwind and upwind of regions of relatively warmer air. These warmer air regions are the same that appear in the vertical fields shown in Fig. 3, and are associated with ejection events. The horizontal field of conditionally averaged vorticity (Fig. 6a) for the forward-scatter events shows two pairs of counter-rotating vortices on either side of the center-spanwise line on which the SFS dissipation events occur (at x'=0 m, y=0 m). Note that the dominant pair of vortices is downwind of the forward-scatter events. Around the backscatter events (Fig. 6b), the dominant vortex pair is shifted with respect to the pair in the forward-scatter events (Fig. 6a) and is located upwind of the backscatter event.

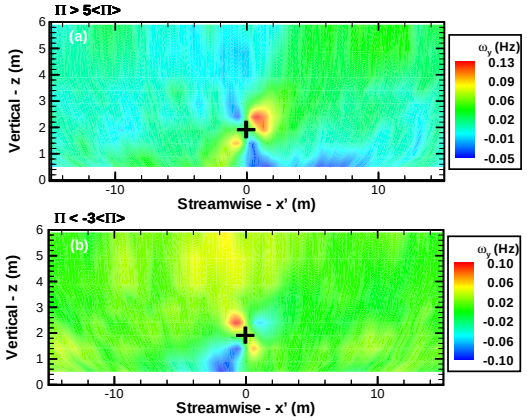

FIG. 4: Vertical fields of conditionally averaged spanwise vorticity, ω_y (Hz), for (a) positive and (b) negative SFS dissipation rates of energy under weakly-unstable conditions. The '+' indicates the location at which the SFS dissipation rates satisfy the threshold condition.

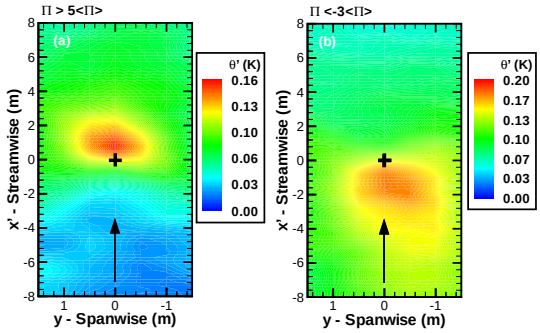

FIG. 5: Horizontal fields of conditionally averaged temperature fluctuations, θ' (K), for positive (left) and negative (right) SFS dissipation rates of energy under weakly unstable conditions. Flow is from bottom to top. The '+' indicates the location at which the SFS dissipation rates satisfy the threshold condition.

The conditionally averaged plots presented here (Figs. 3-6) are based on thousands of realizations of the turbulent flow and are highly indicative of a fundamental coherent structure characterized by the outline of the vorticity contours. For a more detailed understanding and explanation of these contour patterns, we consider previous experimental studies of coherent structures in lower (moderate) Reynolds-number boundary layers (Robinson, 1991; Adrian *et al*, 2000). Conceptual models from these experimental results suggest that coherent structures in the logarithmic layer have hairpin-like structures with characteristic inclined legs that have opposite rotations, extending upward and meeting to form a head of spanwise vorticity. Our results agree with these conceptual models as one can trace out the silhouette of hairpin vortices in our conditionally averaged fields (both vertical

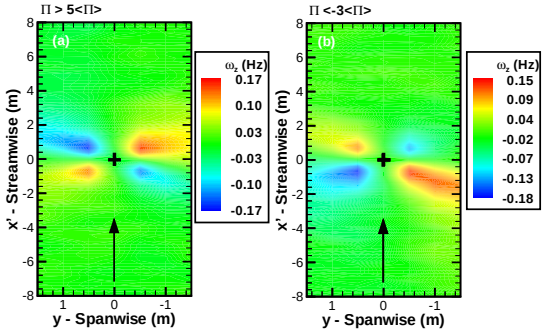

FIG. 6: Horizontal fields of conditionally averaged vertical vorticity, ω_z (Hz), for positive (left) and negative (right) SFS dissipation rates of energy under weakly unstable conditions. Flow is from bottom to top. The '+' indicates the location at which the SFS dissipation rates satisfy the threshold condition.

and horizontal). The rotation of the core of the vortices in the horizontal field agrees with two downward extending legs that have opposite signs of vorticity and directly contribute to the ejection events shown in the velocity field of Fig. 3. Based on our results, a conceptual model is proposed (Fig. 7) that positions strong positive SFS dissipation (again forward-scatter) events on the upper trailing edge of hairpin-like structures and the negative SFS dissipation events (backscatter) on the lower leading edge of the same hairpin-like structures.

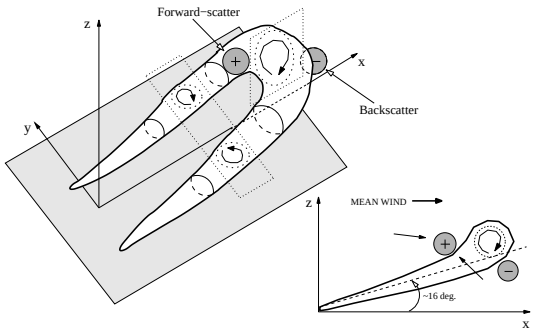

FIG. 7: Conceptual model relating strong positive (+) and negative (-) SFS dissipation events to different regions (shaded) around a hairpin-like coherent structure. The thick solid lines outline an isosurface of vorticity with rotation indicated. The dotted lines indicate the planes on which the conditionally averaged fields are reported.

4. ATMOSPHERIC STABILITY EFFECTS

The effect of atmospheric stability on the inclination of the conditionally averaged structures as observed in Figs. 3-6 is considered here using two different time periods: one during weakly-stable conditions ($z/L = +0.10$) and the other during unstable (convective) conditions ($z/L = -2.39$). Fig. 8 shows vertical fields of conditionally averaged vorticity for each of these periods. The inclina-

tion of the conditionally averaged structure during positive bouyancy (unstable time period) is substantially greater than that for the weakly-stable time period.

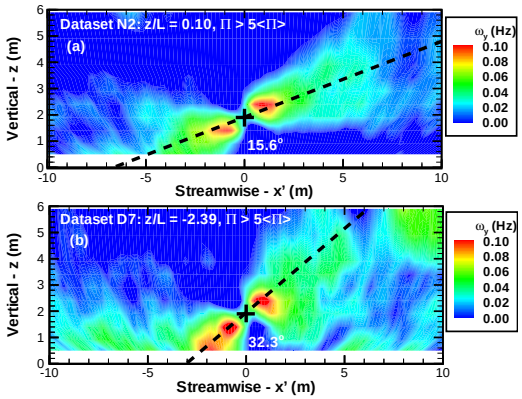

FIG. 8: Conditionally averaged vorticity fields for two different time periods: (a) near-neutral conditions (z/L = +0.10) and (b) convective conditions (z/L = -2.39). The '+' indicates the location at which the SFS dissipation rates satisfy the threshold condition. The dashed lines correspond to the angles of inclination determined from the two-point correlation analysis.

Characteristic inclination angles of structures in the flow have also been quantified using two-point correlations calculated between the streamwise velocity time series along the vertical array. These angles varied between 15 and 35 degrees and are found to be a function of stability. Under near-neutral conditions, the characteristic angle is approximately 16 degrees, which is in good agreement with previous studies in moderate-Reynolds-number flows. From visual inspection, the angle of inclination of the conditionally averaged vorticity contours matches well with values obtained from the peak correlations (shown as dashed lines in Fig. 8).

5. CONCLUSIONS

In the context of LES, we present unique experimental evidence from the atmospheric surface layer of the qualitative role of coherent structures (using information in three directions) on the local intermittent transfers (forward-scatter and backscatter) of energy and scalar variance between resolved and subfilter scales. Strong forward-scatter events are found to be associated with the upper-trailing edge of hairpin-like vortices at convergences in the flow, whereas strong backscatter events are found to be associated with the lower-leading edge of the same type of hairpin vortices and at divergences in the flow. During convective (unstable) conditions, positive buoyancy forces the characteristic angle of the structures to be larger than during weakly-stable conditions.

This information is suitable to be used in *a posteriori* studies to evaluate the performance of current and newly developed SFS models based on their ability to capture the local structure and dynamics of the flow. Our work also complements analytical and conceptual models of the fundamental structures of turbulent boundary layers which may lend guidance to the development of improved SFS parameterizations.

ACKNOWLEDGEMENTS

We would like to thank Marc Parlange and Charles Meneveau, and their research group from Johns Hopkins University and also thank Joe Klewicki of the University of Utah. This work has been supported by NSF grant EAR-0094200 and NASA grant NAG5-10569 and computer resources from the Minnesota Supercomputing Institute.

REFERENCES

Adrian R J, Meinhart C D and Tomkins C D 2000 Vortex Organization in the Outer Region of the Turbulent Boundary Layer *J. of Fluid Mech.* **422** 1-54

Carper M A, Porté-Agel F 2004 The Role of Coherent Structures on Subfilter-scale Dissipation Rates of Turbulence Measured in the Atmospheric Surface Layer *submitted to Journal of Turbulence*

Kleissl J, Meneveau C and Parlange M B 2003 On the Magnitude and Variability of Subgrid-Scale Eddy-Diffusion Coefficients in the Atmospheric Surface Layer *J. Atmos. Sci.* **60** 2372-2388

Meneveau C and Katz J 2000 Scale-invariance and Turbulence Models for Large-Eddy Simulation *Annu. Rev. Fluid Mech.* **32** 1-32

Porté-Agel F, Parlange M B, Meneveau C and Eichinger W E 2001a A-priori Field Study of the Subgrid-scale Heat Fluxes and Dissipation in the Atmospheric Surface Layer *J. Atmos. Sci.* **58** 2673-2698

Porté-Agel F, Pahlow M, Meneveau C and Parlange M B 2001b Atmospheric Stability Effect on Subgrid-scale Physics for Large-Eddy Simulation *Adv. Wat. Res.* **24** 1085-1102

Robinson S K 1991 Coherent Motion in the Turbulent Boundary Layer *Annu. Rev. Fluid Mech.* **23** 601-639

Sullivan P P, Horst T W, Lenschow D H, Moeng C-H and Weil J C 2003 Structure of subfilter-scale fluxes in the atmospheric surface layer with application to large-eddy simulation modelling *J. Fluid Mech.* **482** 101-139